

System Size and Flavour Dependence of Chemical Freeze-out Temperatures in ALICE pp, pPb and PbPb Collisions at LHC Energies

Fernando Antonio Flor, Gabrielle Olinger, René Bellwied
Department of Physics, University of Houston, Houston, Texas 77204, USA

Abstract

We present the system size and flavour dependence of the chemical freeze-out temperature (T_{ch}) at vanishing baryo-chemical potential calculated via thermal fits to experimental yields for several centrality classes in pp, pPb and PbPb collisions measured by ALICE. Using the Thermal-FIST Hadron Resonance Gas model package, we compare the quality of fits across various treatments of strangeness conservation under different freeze-out conditions as a function of the charged particle multiplicity density ($\langle dN_{\text{ch}}/d\eta \rangle$). Additionally, we examine how the anti-hadron to pion yield ratios of light and strange baryons, as well as the ϕ meson, evolve within a flavour-dependent model. Through a unique two-temperature chemical-freezeout approach, we show that flavour dependence of T_{ch} leads to a natural explanation of strangeness enhancement from small to large systems at LHC energies without requiring any canonical suppression for small $\langle dN_{\text{ch}}/d\eta \rangle$.

Keywords: Strangeness Enhancement, Sequential Flavour Freeze-out, Statistical Hadronization, Hadron Resonance Gas

1. Introduction

Hadronization and chemical freeze-out have been suggested to coincide at the phase boundary in the Quantum Chromodynamics (QCD) phase diagram based on results from Statistical Hadronization Models (SHMs) using particle yields measured at the Large Hadron Collider (LHC) and the Relativistic Heavy Ion Collider (RHIC), when compared to pseudo-critical temperature calculations from temperature dependent continuum extrapolations of the chiral susceptibilities on the lattice [1, 2, 3, 4, 5]. A point of interest emerges concerning whether the phase transition from quark to hadron degrees of freedom occurs at the same temperature for all particle species and/or quark flavours.

Final state particle yields have been successfully reproduced by SHMs to nine orders of magnitude over a wide energy range in high energy collisions of heavy ions [6, 7]. SHMs typically use experimental hadron yields from central events (0 - 10%) in relativistic heavy ion collisions as an anchor for determining common freeze-out parameters in the QCD phase diagram – namely, the chemical freeze-out temperature (T_{ch}) and the baryo-chemical potential (μ_{B}) – within a Grand Canonical Ensemble (GCE), where baryon number, electric charge and strangeness are conserved on average.

The GCE treatment has been shown to inadequately reproduce experimental results in a centrality dependent manner across pp, pPb and PbPb collision systems measured by the ALICE

Collaboration – particularly where $\langle dN_{\text{ch}}/d\eta \rangle \leq 20$ [8]. The aforementioned is often attributed to the presence of canonical suppression in the smaller systems and may be partially remedied by employing a Strangeness Canonical Ensemble (SCE), in which strangeness is explicitly conserved within some correlation volume V_{C} using a single value of T_{ch} for all particle species (1CFO). The question arises as to whether additional canonical strangeness suppression in small systems provides an adequate description of the overall production of final state (multi)strange hadrons as measured at LHC energies. The presence of such a suppression, commonly represented by a strangeness saturation parameter (γ_{S}) within the fireball volume of hadronic collisions, is known to decrease with increasing collision energy [9, 10].

Thus, canonical strangeness suppression scaling as an inverse function of collision energy can be equated with an increasing value of γ_{S} . At LHC energies, γ_{S} is expected to be asymptotic to unity [8, 11], i.e. full saturation of strangeness is achieved. The dominating presence of strangeness enhancement at ALICE, even in small systems, is evident from an energy dependent comparison of final state anti-hadron to π^+ yields measured by ALICE and STAR [12], where production of strange baryons is fully saturated for collision energy values above $\sqrt{s_{\text{NN}}} = 62.4$ GeV.

Nevertheless, in order to fully describe the experimental data, further considerations are made regarding the interplay between V_{C} , the fireball volume (V), the experimental rapidity window (Δy) and γ_{S} [13, 14]. This letter aims at providing a novel description of strangeness enhancement across all three colli-

Email address: faflor@uh.edu (Fernando Antonio Flor)

sion systems measured by ALICE, assuming full saturation of strangeness is inherently present at LHC energies. Our description of final state hadron yields within the SHM framework relies not on the canonical suppression paradigm, but rather on flavour-dependent freeze-out temperatures and volumes across increasing $\langle dN_{\text{ch}}/d\eta \rangle$ values.

2. Sequential Strangeness Freeze-out

Flavour-dependent freeze-out temperatures in the crossover region of the QCD phase diagram have been predicted by continuum extrapolated susceptibilities of single flavour quantum numbers on the lattice [15, 16]. Flavour specific susceptibility ratios χ_4/χ_2 , suggested as an observable for directly determining freeze-out temperatures [17], show a deviation of the lattice and Hadron Resonance Gas (HRG) model calculations at the peaks of the lattice data, which occur at flavour-dependent temperatures differing by 15 – 20 MeV from light to strange quarks [16]. Similar temperature differences between the light and strange mesons have also been shown in net-particle fluctuation measurements by the STAR Collaboration [18, 19, 20, 21]. An HRG-based study was also performed in a similar analysis on both off-diagonal and diagonal second order correlators of conserved charges [22].

In a previous letter, at vanishing μ_B , we calculated a light flavour freeze-out temperature $T_L = 150.2 \pm 2.6$ MeV and a strange flavour freeze-out temperature $T_S = 165.1 \pm 2.7$ MeV, by employing the GCE approach to heavy ion collisions within the framework of the Thermal FIST (“The FIST”) HRG model package and varying the particle species included in each thermal fit [23].

In this letter, we extend this flavour-dependent two chemical freeze-out (2CFO) temperature approach to pp, pPb and PbPb collision systems measured by ALICE as a function of increasing $\langle dN_{\text{ch}}/d\eta \rangle$, rendering a natural explanation of strangeness enhancement from small to large systems at vanishing μ_B without further modifying Δy , V_C nor γ_S .

3. Model and Data Preparation

All calculations shown here were performed using the open source “The FIST” thermal model package [24]. In this iteration, we modeled an ideal non-interacting gas of hadrons and resonances within both, the GCE and the SCE scenarios, for the sake of comparison. The analysis was two-fold: to gauge the sensitivity of the chemical freeze-out temperature at vanishing μ_B relative to the ensemble of choice, and to employ a 2CFO treatment onto the reigning ensemble.

As the HRG input list, we used the PDG2016+ hadronic spectrum [25]. The PDG2016+ hadronic spectrum has been shown to be an optimized compromise between too few and

too many resonant states when compared to lattice QCD predictions [25]; it includes a total of 738 states (i.e. *, **, *** and **** states from the 2016 Particle Data Group Data Book [26]).

Yield data for π^+ , π^- , K^+ , K^- , p , \bar{p} , Λ , $\bar{\Lambda}$, Ξ^- , $\bar{\Xi}^+$, Ω^- , $\bar{\Omega}^+$, K_S^0 , and ϕ for ALICE pp collisions at $\sqrt{s} = 7.00$ TeV [27], pPb collisions at $\sqrt{s_{\text{NN}}} = 5.02$ TeV [28, 29, 30] and PbPb collisions at $\sqrt{s_{\text{NN}}} = 2.76$ TeV [31, 32, 33, 34] across all available multiplicity classes were included in our analysis.

Table 1: Available centrality bins and corresponding values of charged particle multiplicity density for ALICE pp collisions at $\sqrt{s} = 7.00$ TeV, pPb collisions at $\sqrt{s_{\text{NN}}} = 5.02$ TeV and PbPb collisions at $\sqrt{s_{\text{NN}}} = 2.76$ TeV. For the pp sample, the multiplicity classes are labelled in accordance to their generalized definitions in [27].

pp at 7.00 TeV		
Multiplicity Class	Centrality Bin	$\langle dN_{\text{ch}}/d\eta \rangle$
I-II	0-5%	17.47 ± 0.524
III-VI	5-28%	10.383 ± 0.313
VII-VIII	28-48%	6.057 ± 0.19
IX-X	48-100%	2.886 ± 0.135
pPb at 5.02 TeV		
	0-5%	45 ± 1
	5-10%	36.2 ± 0.8
	10-20%	30.5 ± 0.7
	20-40%	23.2 ± 0.5
	40-60%	16.1 ± 0.4
	60-80%	9.8 ± 0.2
	80-100%	4.3 ± 0.1
PbPb at 2.76 TeV		
	0-10%	1447.5 ± 54.5
	10-20%	966 ± 37
	20-40%	537.5 ± 19
	40-60%	205 ± 7.5
	60-80%	55.5 ± 3

All throughout, we follow a shorthand notation when naming our fits to (anti)particle species (e.g. Ω refers to both Ω^- and $\bar{\Omega}^+$, etc.), unless explicitly noted otherwise.

In the GCE configuration, the thermal fits were performed with T_{ch} (MeV) and V (fm^3) as free parameters, keeping $\mu_B = 0$ – as is the case at LHC energies – and setting γ_S and γ_q to unity in order to ensure a full saturation of strangeness and electric charge. Systematic HRG-based studies on the determination of the latter three parameters at top LHC energies can be found in Refs. [35, 36]. We focused on varying the particle species included in the fit in order to gauge the sensitivity of T_{ch} to each fit. The particle species included in our flavour-dependent temperature fits were $\pi K p$, $\pi K p \Lambda \Xi \Omega K_S^0 \phi$ and $K \Lambda \Xi \Omega K_S^0 \phi$, hereinafter referred to as “light”, “all” and “strange”, respectively.

Since the kaon yields have been shown to be insensitive to the freeze-out temperature [37], we included them in light fit for the sake of having sufficient degrees of freedom. We compared the extracted T_{ch} values, for the light, strange and all fits, and their corresponding χ^2/dof measures as a function of their $\langle dN_{\text{ch}}/d\eta \rangle$ values across all three collision systems.

In the SCE configuration, our thermal fits were instead performed with T_{ch} (MeV) and V (fm^3) as free parameters, keeping $\mu_B = 0$, $V_C = V$ and setting γ_S and γ_q to unity. Setting $V_C = V$ was done in order to guarantee a local conservation of strangeness within the calculated fireball volume per unit rapidity.

The initial SCE analysis followed the same procedure than the early GCE trial, however, the following procedures were not performed for the GCE approach due to the deterioration of the quality of its fits across all three collision systems. A similar approach was presented in [38, 39], with a notable difference in the manner in which the pion yields were calculated in the thermal model. In our case, the pion, and all other, yields were based on experimental values measured over a single unit of rapidity around mid-rapidity.

For our SCE analysis, the $\pi K p \Lambda \Xi \Omega K_S^0 \phi$ yields were calculated by fixing the temperature to the flavour specific freeze-out temperatures at $\mu_B = 0$ from our original study [23], such that $T_L = 150$ MeV for πp and $T_S = 165$ MeV for $K \Lambda \Xi \Omega K_S^0 \phi$. We calculated the anti-hadron to π^+ ratio as a function of $\langle dN_{\text{ch}}/d\eta \rangle$ and compared our results with the experimental data. The choice of the anti-hadron to π^+ ratio was made, as in [12], in order to use only particles produced during the evolution of the fireball. This will allow us to facilitate future centrality dependent comparisons to lower collision energy measurements, where $\mu_B \neq 0$. In order to explicitly show the temperature dependence of the fireball volumes, we calculated the volumes across all three systems as a function of $\langle dN_{\text{ch}}/d\eta \rangle$ with temperatures fixed to the aforementioned flavour specific temperatures, as well as $T = 158$ MeV for a non-flavour-dependent temperature.

4. Results and Discussion

We extracted freeze-out temperatures T_{ch} via ‘The FIST’ for the light, all, and strange particle thermal fits across increasing $\langle dN_{\text{ch}}/d\eta \rangle$ values for pp, pPb, and PbPb collision systems at ALICE in the GCE and SCE configurations using experimental particle yields.

The top panel of Figure 1 shows the extracted freeze-out temperatures T_{ch} as a function of $\langle dN_{\text{ch}}/d\eta \rangle$ at $|\eta| < 0.5$ for the three different fits within the GCE treatment. The pp, pPb, PbPb points are shown as closed circles, open diamonds and closed squares, respectively. The red, green, and blue points pertain to the extracted T_{ch} values for the light, all, and strange fits, respectively. The coloured bands were determined from the

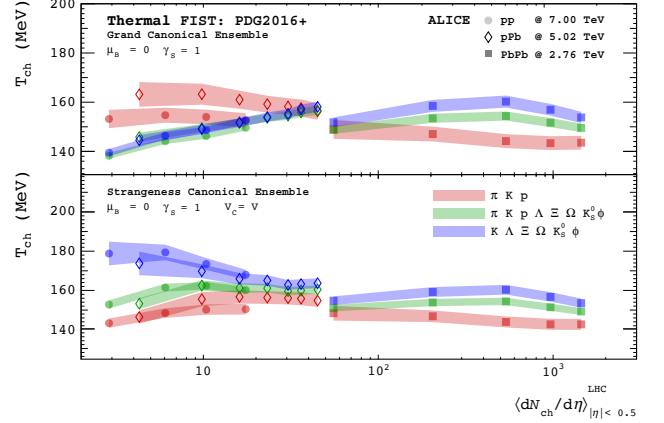


Figure 1: Top Panel: Flavour-dependent ‘The FIST’ GCE Fits to Yields using the PDG2016+ hadronic spectrum for ALICE pp collisions at $\sqrt{s} = 7.00$ TeV, pPb collisions at $\sqrt{s_{\text{NN}}} = 5.02$ TeV and PbPb collisions at $\sqrt{s_{\text{NN}}} = 2.76$ TeV, respectively, shown as as closed circles, open diamonds and closed squares as a function of $\langle dN_{\text{ch}}/d\eta \rangle$. For all fits, $\mu_B = 0$ and $\gamma_S = 1$, while T_{ch} , and V were used as free parameters. Red, green, and blue points represent the light, all, and strange fits, respectively. Bottom Panel: Flavour-dependent ‘The FIST’ SCE Fits to Yields using the PDG2016+ hadronic spectrum for ALICE pp collisions at $\sqrt{s} = 7.00$ TeV, pPb collisions at $\sqrt{s_{\text{NN}}} = 5.02$ TeV and PbPb collisions at $\sqrt{s_{\text{NN}}} = 2.76$ TeV as a function of $\langle dN_{\text{ch}}/d\eta \rangle$. For all SCE fits, $\mu_B = 0$, $\gamma_S = 1$ and $V_C = V$, while T_{ch} , and V were used as free parameters. The bottom panel follows the same labeling convention used in the top panel.

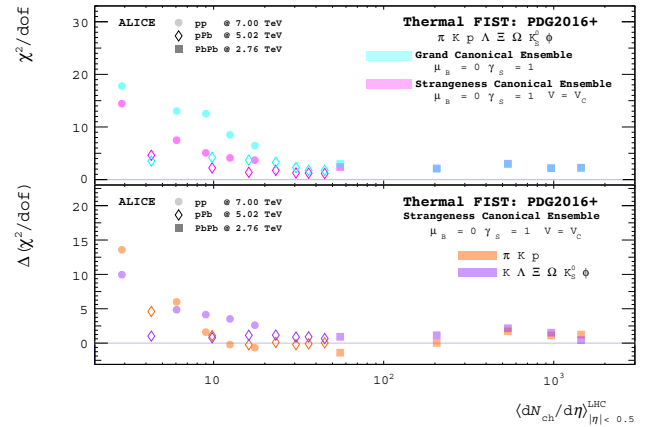


Figure 2: Top Panel: ‘The FIST’ χ^2/dof values of the GCE (cyan) and SCE (magenta) fits used in the all fits of the top and bottom panels of Figure 1, respectively, using the PDG2016+ hadronic spectrum for ALICE pp collisions at $\sqrt{s} = 7.00$ TeV, pPb collisions at $\sqrt{s_{\text{NN}}} = 5.02$ TeV and PbPb collisions at $\sqrt{s_{\text{NN}}} = 2.76$ TeV as a function of $\langle dN_{\text{ch}}/d\eta \rangle$. Bottom Panel: ‘The FIST’ $\Delta(\chi^2/\text{dof})$ values for the SCE fits used in the light (orange) and strange (purple) fits of the bottom panel of Figure 1 via the PDG2016+ hadronic spectrum for ALICE pp collisions at $\sqrt{s} = 7.00$ TeV, pPb collisions at $\sqrt{s_{\text{NN}}} = 5.02$ TeV and PbPb collisions at $\sqrt{s_{\text{NN}}} = 2.76$ TeV as a function of $\langle dN_{\text{ch}}/d\eta \rangle$. For both the top and bottom panels, the corresponding χ^2/dof and $\Delta(\chi^2/\text{dof})$ values for pp, pPb and PbPb collision systems are respectively shown as as closed circles, open diamonds and closed squares.

propagation of the error of the fits onto the freeze-out parameters. The bottom panel of Figure 1 shows the extracted freeze-out temperatures T_{ch} as a function of $\langle dN_{\text{ch}}/d\eta \rangle$ at $|\eta| < 0.5$ for the three different fits within the SCE treatment, following the same labeling convention as in the top panel of the figure. Qualitatively contrasting both top and bottom panels, we observe a deterioration of the flavour-dependent 2CFO approach occurring in the pp and pPb systems when using the GCE scenario, starting at values of $\langle dN_{\text{ch}}/d\eta \rangle < 50$. This is not the case in the SCE treatment, where a flavour-dependent temperature separation is consistently present as a function of $\langle dN_{\text{ch}}/d\eta \rangle$ across all three systems. It also is worth noting that in the grand canonical limit, i.e. for values of $\langle dN_{\text{ch}}/d\eta \rangle > 50$, both the GCE and SCE treatments render almost identical T_{ch} values. Nevertheless, in order to qualitatively differentiate between the two treatments, we performed an in-depth comparison of the fit quality of the aforementioned T_{ch} values as a function of $\langle dN_{\text{ch}}/d\eta \rangle$, which is separately shown in Figure 2.

The top panel of Figure 2 depicts the corresponding χ^2/dof values for the GCE and SCE all fits of the top and bottom panels of Figure 1, shown in cyan and magenta, respectively. The pp, pPb, PbPb points are shown as closed circles, open diamonds and closed squares. In the large system (PbPb), we observe a consistent quality of fit for all multiplicity classes in the GCE and SCE scenarios, with almost identical values for both approaches. However, in the GCE case, we observe a deteriorating quality of fits in the small systems (pp and pPb), with $\chi^2/\text{dof} > 5$ for nearly all fits to pp data. This renders an inconsistent description of temperatures across multiplicity within the GCE treatment of smaller systems. Instead, using the SCE approach, we observe a consistent quality of fit, specifically, $\chi^2/\text{dof} \lesssim 5$, across all small and large systems with corresponding values $\langle dN_{\text{ch}}/d\eta \rangle \geq 10$.

The bottom panel of Figure 2 shows the $\Delta(\chi^2/\text{dof})$ values corresponding to the SCE fits performed in the light and strange fits from the bottom panel of Figure 1 – shown in orange and purple, respectively. As in the top panel, the pp, pPb, PbPb points are respectively shown as closed circles, open diamonds and closed squares. The $\Delta(\chi^2/\text{dof})$ values for the orange points in the bottom panel of Figure 2 were calculated as the difference between the corresponding χ^2/dof values of the SCE all (green) fits and the SCE light (red) fits from the bottom panel in Figure 1. Similarly, the $\Delta(\chi^2/\text{dof})$ values for the purple points in the bottom panel of Figure 2 were calculated as the difference between the corresponding χ^2/dof values of the SCE all (green) fits and the SCE strange (blue) fits from the bottom panel in Figure 1. This procedure was done in order to explicitly discriminate between notable differences in the quality of the fits when employing the 2CFO approach within the SCE, where any improvements of the fit quality would render $\Delta(\chi^2/\text{dof})$ values approximately equal to the magenta χ^2/dof values shown in the

top panel. Conversely, any $\Delta(\chi^2/\text{dof})$ values below zero reflect a worsened fit quality. We note that for all three systems, across all values of $\langle dN_{\text{ch}}/d\eta \rangle$, the calculated $\Delta(\chi^2/\text{dof})$ values for both the light (orange) and strange (purple) points generally follow the same trend as the all (cyan) points in the top panel. Without loss of generality, this suggests an overall improvement of the fits when employing the flavour-dependent 2CFO approach in the SCE treatment. The presence of negative $\Delta(\chi^2/\text{dof})$ values can only be seen for a few of the light fits and can be attributed to a decreasing number of degrees of freedom, which causes an overall increase in the calculated χ^2/dof . Moreover, the final χ^2/dof values for the flavour specific fits can be obtained by subtracting the values in the lower panel from the magenta points in the upper panel of Figure 2. One can thus observe a consistent quality of fit – specifically, $\chi^2/\text{dof} \lesssim 5$ – for each of the three types of fits across the small and large systems with corresponding values of $\langle dN_{\text{ch}}/d\eta \rangle \geq 10$. We note that the quality of fit is consistent for both the light and strange fits to a lower corresponding value of $\langle dN_{\text{ch}}/d\eta \rangle \geq 5$. Generally, the χ^2/dof values for the light and strange fits are lower than those for the all fit.

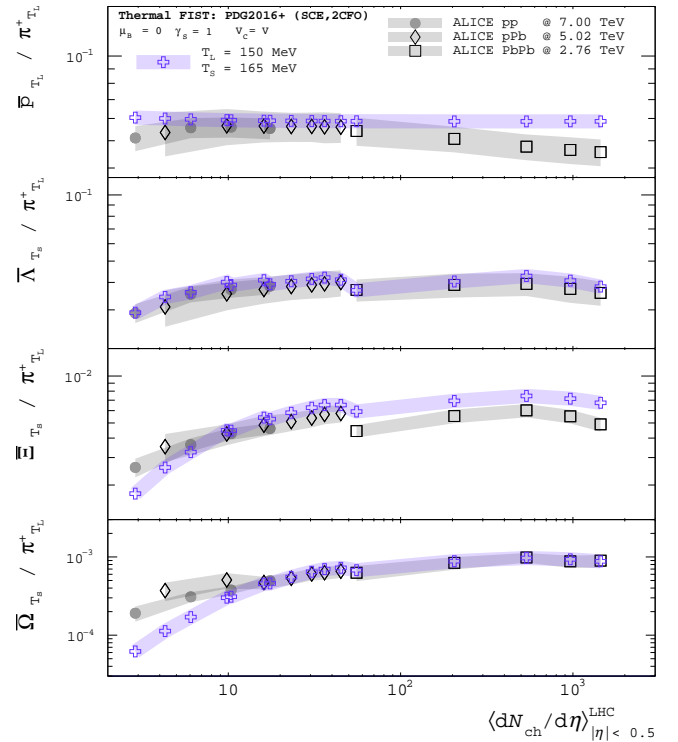


Figure 3: 2CFO SCE ‘The FIST’ Thermal Model anti-hadron to π^+ yield ratio calculations via the PDG2016+ hadronic spectrum for ALICE pp collisions at $\sqrt{s} = 7.00$ TeV, pPb collisions at $\sqrt{s_{\text{NN}}} = 5.02$ TeV, and PbPb collisions at $\sqrt{s_{\text{NN}}} = 2.76$ TeV as a function of $\langle dN_{\text{ch}}/d\eta \rangle$. From top to bottom: \bar{p}/π^+ , $\bar{\Lambda}/\pi^+$, Ξ/π^+ , and Ω/π^+ , respectively. ALICE experimental points for pp, pPb and both PbPb collision systems are respectively shown as grey closed circles, black open diamonds and black closed squares. Purple open crosses depict to our calculated SCE 2CFO anti-hadron to π^+ ratios at vanishing baryo-chemical potential in the SCE framework based on the flavour specific temperatures extracted in [23]. For all calculations, $\mu_B = 0$, $\gamma_S = 1$ and $V_C = V$.

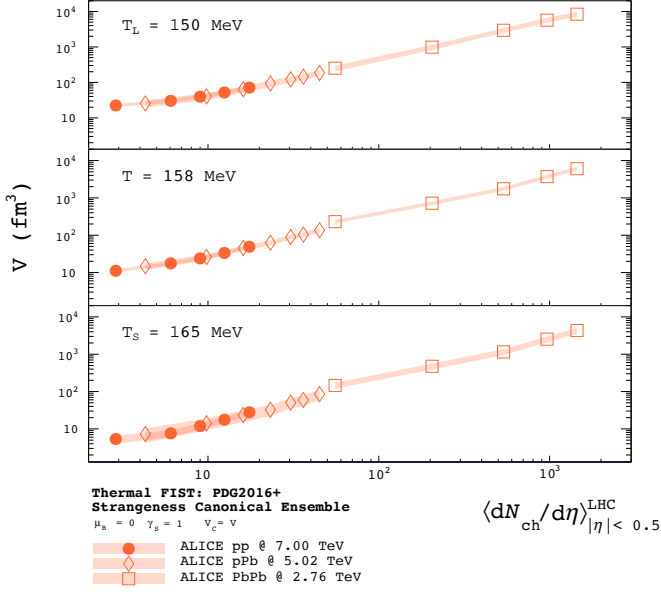


Figure 4: ‘The FIST’ SCE Thermal Model temperature dependent volume per unit rapidity calculations via the PDG2016+ hadronic spectrum for ALICE pp collisions at $\sqrt{s} = 7.00$ TeV, pPb collisions at $\sqrt{s_{NN}} = 5.02$ TeV, and PbPb collisions at $\sqrt{s_{NN}} = 2.76$ TeV as a function of $\langle dN_{ch}/d\eta \rangle$ based on the flavour specific temperatures extracted in [23]. From top to bottom: Volume determinations at 150 MeV, 158 MeV and 165 MeV. Our calculated volumes per unit rapidity of pp, pPb and both PbPb collision systems are respectively shown as grey orange circles, orange open diamonds and orange closed squares. For all calculations, $\mu_B = 0$, $\gamma_S = 1$ and $V_C = V$.

Figure 3 shows the anti-hadron to π^+ ratio as a function of $\langle dN_{ch}/d\eta \rangle$, starting from the top panel down to the bottom: \bar{p}/π^+ , $\bar{\Lambda}/\pi^+$, $\bar{\Xi}/\pi^+$ and $\bar{\Omega}/\pi^+$, respectively. The experimental points for ALICE pp, pPb and both PbPb collision systems are shown as grey closed circles, black open diamonds and black closed squares, respectively. The purple open crosses indicate our calculated 2CFO anti-hadron to π^+ ratios within the SCE framework in ‘The FIST’ using the flavour specific temperatures $T_L = 150$ MeV for π^+ and \bar{p} , and $T_S = 165$ MeV for $\bar{\Lambda}$, $\bar{\Xi}$ and $\bar{\Omega}$. The corresponding model calculations of the ϕ to π^+ ratio are shown separately in Figure 5, keeping the same purple cross colour convention, for the traditional treatment of net-strangeness of the ϕ meson of $S = 0$. For this study we chose the chemical temperatures extracted in our previous letter [23] for central (0 - 10%) PbPb collisions at $\mu_B = 0$ across all centralities and system sizes. We also tested that using instead the temperatures shown in the bottom panel of Figure 1 will not make a difference in final state particle yield ratios since a simultaneous change in volume from the values shown in Figure 4 will compensate any temperature differences.

Our results show an excellent agreement with the experimental yield ratios measured by ALICE across all three systems and are consistent with those shown by [38, 39]. Early calculations [40] requiring an additional canonical suppression factor, i.e. $\gamma_S < 1$, can be excluded based on our studies and Ref. [39].

At these high collision energies, strangeness seems saturated even in the smallest systems. The main differences to Ref. [39] emerge from the fact that our results do not require different rapidity windows for pions and strange particles and no additional normalization factor was used to reproduce the experimental results. In our analysis, the accurate representation of final state particle yields relies solely on the use of flavour-dependent temperatures and fireball volumes – the relevant volumes as a function of $\langle dN_{ch}/d\eta \rangle$ as determined by the model are shown in Figure 4.

Lastly, we varied the treatment of net-strangeness of the ϕ meson in our model between $S = 0$, $S = 1$ and $S = 2$ to gauge the sensitivity of the calculated yields and to elucidate the question of strangeness enhancement in the case of the vector meson. Figure 5 shows the ϕ to π^+ ratio as a function of $\langle dN_{ch}/d\eta \rangle$, following the same labeling convention for experimental points and 2CFO thermal model calculations as Figure 3, using an ad hoc variation of the total strangeness (S) value within the model for the ϕ meson. To reiterate, the π^+ and ϕ values were calculated at $T_L = 150$ MeV and $T_S = 165$ MeV, respectively. For the comparison to the data, we arbitrarily fixed the total strangeness of the ϕ meson to $S = 0$ (purple open crosses), $S = 1$ (cyan open crosses) and $S = 2$ (magenta open crosses), respectively.

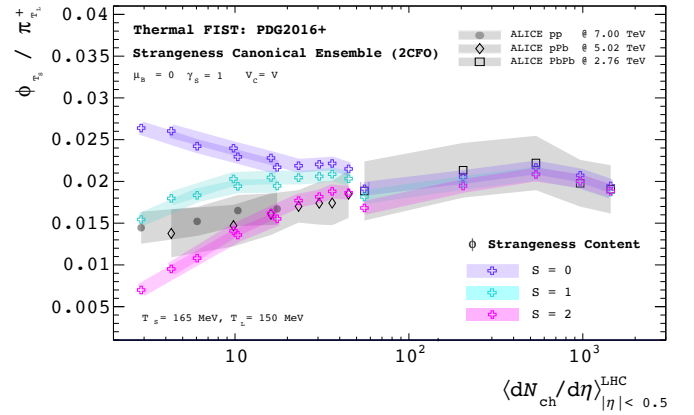


Figure 5: 2CFO SCE ‘The FIST’ Thermal Model ϕ to π^+ yield ratio calculations via the PDG2016+ hadronic spectrum for ALICE pp collisions at $\sqrt{s} = 7.00$ TeV, pPb collisions at $\sqrt{s_{NN}} = 5.02$ TeV, and PbPb collisions at $\sqrt{s_{NN}} = 2.76$ TeV as a function of $\langle dN_{ch}/d\eta \rangle$. ALICE experimental points for pp, pPb, PbPb collisions are respectively shown in grey as closed circles, open diamonds, and closed squares. Purple, cyan and magenta open crosses depict our calculated SCE 2CFO ϕ to π^+ ratios in the SCE framework based on the flavour specific freeze-out temperatures at vanishing baryo-chemical potential shown in [23] fixing the total strangeness values for the ϕ meson to $S = 0$, $S = 1$ and $S = 2$, respectively. For all calculations, $\mu_B = 0$, $\gamma_S = 1$ and $V_C = V$.

In the case of $S = 0$, the calculated yield ratios are well described by the 2CFO approach only in the large systems, for $\langle dN_{ch}/d\eta \rangle > 50$. Our model vastly overestimates the value of the ratio for both the pp and pPb systems. In the case $S =$

1, we see an improvement particularly in the smaller systems, with our calculated values almost falling within the errors of the experimental data for all multiplicity bins. Lastly, for the case of $S = 2$, the model underestimates the experimental yield ratios for values of $\langle dN_{\text{ch}}/d\eta \rangle < 10$, but does otherwise quite well. Our results suggest that for ϕ production in small systems the ϕ should not be considered a $S = 0$ particle, because simple flavor conservation and recombination arguments require more than a single string to fragment to form an $s\bar{s}$ state. Therefore, ϕ yields can be more accurately calculated, within the HRG framework, by assuming a strangeness content between 1 and 2.

5. Conclusion

We presented determinations of freeze-out temperatures T_{ch} for the light, full, and strange particle thermal fits across increasing $\langle dN_{\text{ch}}/d\eta \rangle$ values for pp, pPb, and PbPb collision systems at ALICE in the GCE and SCE configurations from experimental particle yields via ‘The FIST’ using the PDG2016+ hadronic spectrum. Moreover, we also showed thermal model anti-hadron to π^+ yield ratio calculations in these same collision systems as a function $\langle dN_{\text{ch}}/d\eta \rangle$, with particular attention given to the treatment of the total strangeness content of the ϕ meson. In the scope of the Strangeness Canonical Ensemble within the framework of the Thermal FIST HRG model package, we show an excellent description of experimental yield ratios across all three systems, measured by the ALICE Collaboration as a function of $\langle dN_{\text{ch}}/d\eta \rangle$ at LHC energies, when employing flavour-dependent chemical freeze-out temperatures under the assumption of fully saturated strangeness. In conclusion, the flavour-dependent (T_{ch}) separation established in heavy ion collisions, seems to prevail also at low $\langle dN_{\text{ch}}/d\eta \rangle$ values corresponding to the pp and pPb systems. This sustained separation may also be seen as an indication of QGP formation in small systems.

6. Acknowledgments

The authors acknowledge fruitful discussions with Volodymyr Vovchenko, Claudia Ratti, Paolo Parotto, Jamie Stafford, Livio Bianchi, Boris Hippolyte, Horst Sebastian Scheid and Dhevan Gangadharan. This work was supported by the DOE grant DEFG02-07ER4152. F.A.F. acknowledges ongoing support from the Franco-American Fulbright Commission.

References

- [1] J. Stachel, A. Andronic, P. Braun-Munzinger, and K. Redlich, *Journal of Physics: Conference Series* **509**, 012019 (2014).
- [2] A. Bazavov *et al.* (HotQCD Collaboration), *Phys. Rev. D* **90**, 094503 (2014).
- [3] S. Borsányi, Z. Fodor, C. Hoelbling, S. D. Katz, S. Krieg, and K. K. Szabó, *Physics Letters B* **730**, 99 (2014).
- [4] S. Borsányi, Z. Fodor, C. Hoelbling, S. D. Katz, S. Krieg, C. Ratti, and K. K. Szabó, *Journal of High Energy Physics* **2010**, 73 (2010).
- [5] R. Bellwied, S. Borsányi, Z. Fodor, J. Günther, S. Katz, C. Ratti, and K. Szabó, *Physics Letters B* **751**, 559 (2015).
- [6] J. Cleymans and K. Redlich, *Phys. Rev. Lett.* **81**, 5284 (1998).
- [7] A. Andronic, P. Braun-Munzinger, K. Redlich, and J. Stachel, *Nature* **561**, 321 (2018).
- [8] N. Sharma, J. Cleymans, B. Hippolyte, and M. Paradza, *Phys. Rev. C* **99**, 044914 (2019).
- [9] A. Tounsi and K. Redlich, (2001), arXiv:hep-ph/0111159.
- [10] A. Tounsi, A. Mischke, and K. Redlich, *Nuclear Physics A* **715**, 565c (2003), quark Matter 2002.
- [11] R. Sahoo and D. Biswas, *Adv. High Energy Phys.* **2021**, 6611394 (2021).
- [12] R. Bellwied, *EPJ Web Conf.* **171**, 02006 (2018).
- [13] V. Vovchenko, B. Dönigus, and H. Stoecker, *Phys. Rev. C* **100**, 054906 (2019).
- [14] J. Adam *et al.*, *Physics Letters B* **758**, 389 (2016).
- [15] C. Ratti, R. Bellwied, M. Cristoforetti, and M. Barbaro, *Phys. Rev. D* **85**, 014004 (2012).
- [16] R. Bellwied, S. Borsanyi, Z. Fodor, S. D. Katz, and C. Ratti, *Phys. Rev. Lett.* **111**, 202302 (2013).
- [17] F. Karsch, *Central European Journal of Physics* **10**, 1234 (2012).
- [18] L. Adamczyk *et al.* (STAR Collaboration), *Phys. Rev. Lett.* **112**, 032302 (2014).
- [19] R. Bellwied, J. Noronha-Hostler, P. Parotto, I. Portillo Vazquez, C. Ratti, and J. M. Stafford, *Phys. Rev. C* **99**, 034912 (2019).
- [20] M. Bluhm and M. Nahrgang, *Eur. Phys. J. C.* **79**, 155 (2019).
- [21] J. Adam *et al.* (STAR), *Phys. Rev. C* **102**, 024903 (2020), arXiv:2001.06419 [nucl-ex].
- [22] R. Bellwied, S. Borsányi, Z. Fodor, J. N. Guenther, J. Noronha-Hostler, P. Parotto, A. Pásztor, C. Ratti, and J. M. Stafford, *Phys. Rev. D* **101**, 034506 (2020).
- [23] F. A. Flor, G. Olinger, and R. Bellwied, *Physics Letters B* **814**, 136098 (2021).
- [24] V. Vovchenko and H. Stoecker, *Computer Physics Communications* **244**, 295 (2019).
- [25] P. Alba, R. Bellwied, S. Borsányi, Z. Fodor, J. Günther, S. D. Katz, V. Mantovani Sarti, J. Noronha-Hostler, P. Parotto, A. Pásztor, I. P. Vazquez, and C. Ratti, *Phys. Rev. D* **96**, 034517 (2017).
- [26] C. Patrignani *et al.* (Particle Data Group), *Chin. Phys.* **C40**, 100001 (2016).
- [27] J. Adam *et al.* (ALICE Collaboration), *Nature Phys* **13**, 535 (2017).
- [28] B. Abelev *et al.*, *Phys. Lett. B* **728**, 25 (2014).
- [29] J. Adam *et al.*, *Eur. Phys. J* **76**, 245 (2016).
- [30] J. Adam *et al.*, *Physics Letters B* **758**, 389 (2016).
- [31] B. Abelev *et al.* (ALICE Collaboration), *Phys. Rev. C* **88**, 044910 (2013).
- [32] B. Abelev *et al.* (ALICE Collaboration), *Phys. Rev. Lett.* **111**, 222301 (2013).
- [33] B. Abelev *et al.* (ALICE Collaboration), *Phys. Rev. C* **91**, 024609 (2015).
- [34] B. Abelev *et al.* (ALICE Collaboration), *Physics Letters B* **728**, 216 (2014).
- [35] S. Bhattacharyya, D. Biswas, S. K. Ghosh, R. Ray, and P. Singha, *Phys. Rev. D* **100**, 054037 (2019).
- [36] S. Bhattacharyya, D. Biswas, S. K. Ghosh, R. Ray, and P. Singha, *Phys. Rev. D* **101**, 054002 (2020).
- [37] D. Magestro, *Journal of Physics G: Nuclear and Particle Physics* **28**, 1745 (2002).
- [38] S. Acharya *et al.* (ALICE Collaboration), *Phys. Rev. C* **99**, 024906 (2019).
- [39] V. Vislavicius and A. Kalweit, (2019), arXiv:1610.03001 [nucl-ex].
- [40] S. Chatterjee, A. K. Dash, and B. Mohanty, *J. Phys. G* **44**, 105106 (2017).